Real-time adaptive methods for treatment of mobile organs by MRI-controlled high-intensity focused ultrasound

Baudouin Denis de Senneville, Charles Mougenot, Chrit Moonen

R2.1

Real time adaptive methods for treatment of mobile organs by MRI controlled High Intensity Focused Ultrasound

Baudouin Denis de Senneville*[,1,2], Charles Mougenot*[,1,3], Chrit T.W. Moonen[1]

[1] Laboratory for Molecular and Functional Imaging: From Physiology to Therapy, ERT CNRS/Université Bordeaux 2, 146 rue Léo Saignat, F - 33076 Bordeaux

[2] LaBRI, UMR 5800 CNRS/Université Bordeaux 1 – 351, cours de la Liberation, F - 33405 Talence

[3] Philips Systèmes Médicaux, 64 rue Carnot, F – 92156 Suresnes

* Both authors have contributed equally

Address correspondence to:
C.T.W. Moonen
Imagerie Moléculaire et Fonctionnelle, ERT CNRS
Université « Victor Segalen » Bordeaux 2
146 rue Leo Saignat, case 117
33076 Bordeaux, France

E-Mail: chrit.moonen@imf.u-bordeaux2.fr
Tel: +33 5 57 57 45 92
Fax: +33 5 57 57 45 97

Acknowledgements: European Union, NoE "Diagnostic Molecular Imaging"; Ligue National Contre le Cancer, Conseil Régional d'Aquitaine, Philips Medical Systems, CDTU canceropôle network

Word count : 8659

Abstract

Focused ultrasound is a unique and non-invasive technique for the local deposition of thermal energy deep inside the body. MRI guidance offers the additional benefits of excellent target visualization and continuous temperature mapping. However, treating a moving target poses severe problems because 1) motion related thermometry artifacts must be corrected, 2) the ultrasound focal point must be relocated according to the target displacement. In this paper, a complete MRI compatible High Intensity Focused Ultrasound (HIFU) system is described together with adaptive methods allowing continuous MR thermometry and therapeutic ultrasound with real-time tracking of a moving target, on-line motion correction of the thermometry maps, and regional temperature control based on the Proportional, Integral, and Derivative method. The hardware is based on a 256 element Phased-Array transducer with rapid, electronic, displacement of the focal point. The exact location of the target during ultrasound firing is anticipated using automatic analysis of periodic motions. The methods were tested with moving phantoms undergoing either rigid body or elastic periodical motions. The results show accurate tracking of the focal point. Focal and regional temperature control is demonstrated with a performance, similar to thatobtained with stationary phantoms.

Keywords: HIFU, MRI, mobile organ, temperature mapping, motion correction

Introduction

R1.1

R2.2

R2.3

High Intensity Focused Ultrasound (HIFU) is a non-invasive technique for local thermal therapy (1,2,3,4,5). It is based on oscillating pressure waves with a wavelength of approximately 1 mm that can be concentrated into a focal point with a size depending on ultrasound frequency, focal length and aperture of the transducer. During the wave propagation across tissue, part of the ultrasound energy is absorbed leading to increase of temperature and eventually to cellular necrosis (6,7). The combination of focused ultrasound and MRI (MR-HIFU) is especially promising since MRI allows a high precision of target localization and it is the only noninvasive imaging technique that has been shown to allow accurate temperature mapping in vivo (8,9,10,11). A large range of applications of MR-HIFU has been demonstrated in the clinical field, e.g. in ablation of breast tumors (4,12,13) and uterine fibroids (3,14,15) and in preclinical studies on gene therapy (16), and for local drug delivery (17). MR-HIFU has shown great potential in improved therapeutic precision, and towards cost reduction.

R1.2

R2.4

R1.3

For optimal treatment, temperature in the targeted volume should be controlled accurately and continuously. To obtain such a control, it has been shown that MR thermometry can be used to provide spatial and temporal temperature feedback control of the HIFU device. Until now, such a control system has been demonstrated for immobilized tissues in vitro and in vivo (18,19,20,21). However, treatment of mobile tissues (e.g. liver and kidney tumors) would add a major new field of MR-HIFU applications. In order to make this possible, the MR-HIFU system must be adapted to take the motion into account, both with respect to positioning of the focal point (target tracking), as well as to correcting for motion artifacts in temperature mapping. Most tissue displacements during such interventions are due to periodical motions (induced by respiratory or cardiac activity). Such motions may be treated as rigid motion (translation and rotation) but this may be insufficient because of the elasticity of the organ leading to deformation during motion.

R2.6

MR temperature information is obtained using the temperature dependency of the Proton Resonance Frequency (PRF) (22) according to the following equation for phase changes in RF spoiled, gradient echo sequences (23,24):

R1.4

$$\Delta T = \frac{\Delta\varphi}{\gamma.\alpha.B_0.T_E} \qquad [1]$$

This equation assumes that the temperature variation ΔT is proportional to the phase variation $\Delta\varphi$ divided by the magnetic field intensity B_0, the gyromagnetic ratio γ, the echo time T_E and the frequency temperature constant α. Tissue displacements may lead to MR signal phase changes independent of temperature and hence, PRF temperature measurements are highly sensitive to motion artifacts. From the temperature evolution in each voxel the thermal dose can be calculated which is required to predict tissue necrosis (25). Thus, accurate temperature measurements allow to check the HIFU focal point position and to compute the accumulated thermal dose during the treatment for on-line prediction of tissue ablation. The motion sensitivity currently limits MR-HIFU application to organs with small motion amplitudes or to those that are easily immobilized like uterine fibroid (14), muscle (26) and breast (12). When intra-scan motion artifacts are limited by using fast imaging techniques and/or synchronization of image acquisition with the periodic motion (e.g. respiratory gating or navigator echo (27)), image processing can be used to further improve the quality of thermal maps.

Some algorithms developed to correct temperature maps have previously been tested in patient studies on the basis of temperature stability in the absence of heating (28,29). These studies have shown the efficiency of atlas based multiple reference images. The atlas is generated during a preceding "learning phase". Such techniques provide accurate motion estimation and can thus be used to predict the target displacement in periodic motion and to provide information for tracking target tissue. Without such corrections, treatment may be inefficient or may induce unwanted destruction of healthy neighboring tissue. Here, it is shown that a modern, home-built, HIFU system based on a Phased Array ultrasound transducer and rapid electronic displacement of the focal point, in combination with advanced real-time image processing with correction of motion artifacts in temperature mapping, allows tracking of the mobile target during the heating procedure and regional temperature control.

Methods

Focused ultrasound under MR control

A phased array HIFU transducer with a diameter aperture of 96 mm and a focal length of 80 mm, was designed in-house and manufactured by Imasonic SA (Besançon, France). The positioning of the 256 individual elements of 5.8 mm diameter was optimized for minimal

R1.5

R1.7

R2.17

intensity of secondary lobes and compactness of the transducer (30). The system is able to focus an ultrasonic wave at 1.5 MHz in a focal point with a size of 0.8×0.8×3.5 mm³ (-3 dB level) according to acoustic field simulation based on Rayleigh integration. The acoustic pressure and the position of the focal point are adjusted by choosing the amplitude and the phase of electrical signals. The position of the focal point is adjusted electronically over a volume of 15×15×30 mm³ at a rate of 100 ms. The electrical to acoustic signal conversion efficiency of the transducer is 37 % with an impedance adaptation to 50 Ohm. In addition, the loss of the transmission line amounts to 26 %. This efficiency has been measured for each channel with radiation force pressure measurement using a Sartorius balance (precision of 0.1 mg, model CP324S, Goettingen, Germany) and an absorbing target provided by Imasonic (Besançon, France) with an elastic rubber material filled with metallic powder in order to fully absorb the acoustic energy.

Experiments were performed on a Philips 1.5 Tesla Intera clinical scanner (Philips Medical Systems, Best, the Netherlands). A sample holder allowed the US beam to propagate through a water-filled volume from transducer to sample. A receive-only surface coil (92 mm diameter) was positioned parallel to the transducer plane. Demineralized and degassed water has been used at the water-sample interface to avoid air bubbles. The oxygen gas content was 4 mg/l (ppm) as measured with an oxymeter (Consort, France, reference C535).

R2.9

Real-time PRF based MR-thermometry was performed using RF-spoiled, lipid suppressed (using a 1-1 binomial frequency-selective RF pulse), single-shot gradient echo echo-planar sequences. The following acquisition parameters were used: echo time 40.9 ms, repetition time 1 second, slice thickness 4.5 mm. A single slice with a spatial resolution of 128×128 voxels was reconstructed from 96×96 acquired voxels. With a field of view of 192×192×4.5 mm^3, the resulting voxel size is 2×2×4.5 mm^3.

Initial data processing was done by the MR acquisition computer. Real and imaginary data were transferred on-line to the HIFU computer in charge of temperature visualization and control of HIFU driver. This HIFU computer is equipped with an Athlon 3.2 GHz XP processor and 1 GB of RAM running under the Windows XP operating system. From the acquired data set an image registration algorithm estimates organ displacement in an area of interest in order to register images and suppress inter-scan motion artifacts in temperature maps. Briefly, an array of reference images results from the initial "learning phase". The procedure makes it possible to define automatically the position of the focal point in the next firing period in order to focus the deposition of energy in the desired tissue area. The

processing algorithm is derived from previously described procedures and is further elaborated below.

Periodical motions also require accurate timing measurements in order to anticipate the target position due to periodic tissue displacements. A microcontroller at 20 MHz (Microchip Technology Incorporated, reference PIC16F688) keeps track of the start of the MR pulse sequence with a microsecond temporal resolution. This information is transferred to the HIFU therapeutic computer in a few milliseconds.

The position of HIFU focal point and desired power are transferred via optical fibers to an in-house designed 256 channel generator/amplifier, built by Radio Concept Développement et Communication (St Martin de Hinx, France). This generator produces sinusoidal waves using direct digital synthesizer provided by Analog Device (Northwood, England, reference AD9835). Each electrical sinusoidal is amplified with a dual differential linear amplifier manufactured by Texas Instruments (Dallas, United States, reference THS6012). Output signals are isolated with a transformer and filtered using a low pass filter and a 64 MHz reject filter. The electrical signals are then transmitted to the ultrasound phased array transducer via an impedance matching box located next to the magnet cryostat. A specific phase for each channel is produced by direct digital synthesizer components (accuracy 1°) in order to focus the beam at the desired location. The system is designed for a maximum of 180 Watts acoustical power. At the surface of the transducer composed of 256 elements of 26.4 mm², the maximal available acoustical power is 2.7 W/cm².

Evaluation platform

For testing MRI controlled HIFU together with spatial temperature control, a mobile evaluation platform was installed on the patient MRI bed (Figure 1). A plastic bag with fresh pig muscle was installed on the platform. Its displacement was remotely controlled by a mechanical transmission line. The motion period is varied by adjusting the voltage applied to the motor. Also, the motion can be rigid when placed over a sliding support or elastic upon the use of a stopping block. For studying rigid motion, e.g. translation, the position of the transmission line is measured with a millimeter striped bar. Two transceiver optical diodes detect the position of the striped bar with a precision of 0.5 mm. A microcontroller at 20 MHz (Microchip Technology Incorporated, USA, reference PIC16F688) records the number of graduated displacements with a microsecond temporal accuracy. As soon as a graduation change is detected, timing and position of the target are transferred to the HIFU therapeutic

computer by a RS232 connection in few milliseconds. Those real-time target position data are used to quantify the accuracy of the estimated and anticipated displacements derived from MR images.

Theory

Since PRF-based temperature maps result from MR signal phase differences, MRI temperature imaging is highly sensitive to intra-scan and inter-scan motion artifacts. Since single-shot acquisition techniques were used in this study, only inter-scan artifacts have to be corrected. In the following, methods are described to correct such artifacts in temperature maps. Then, the position of the focal point is adjusted in order to track the target displacement. Note that data processing has to be performed rapidly to ensure on-line monitoring of temperature evolution. It implies that image processing has to be done within the update time between two successive acquisitions.

Correction of periodical motion artifacts in temperature maps

As temperature is computed from phase difference (see equation [1]), organ motion induces specific inter-scan thermometry artifacts. Indeed, during a therapeutic intervention of a mobile organ, the main parameters involving phase signal modifications are:

1) the temperature variation induced by the heating of the targeted area;
2) the spatial transformation generated by the displacement of the signal source induced by organ motion;
3) the perturbation generated by the modification of the magnetic susceptibility field induced by organ displacements.

It is hardly feasible to separate those three contributions in a single phase image, and therefore the second and third causes should be removed separately. During the intervention, motion field vectors estimated from anatomical images can be used to correct the spatial transformation in phase images (an outline of this processing step is given in Appendix 1). This process improves the precision of on-line temperature measurement by calculating phase differences for pixels corresponding to identical spatial localization. The measured phase variation (and thus the apparent rise of temperature) is also related to the modification of spatial susceptibility effects (31). The main variations of the magnetic field are located at the

interface of tissues with different susceptibility. The influence of susceptibility variation on the measured phase signal depends on imaging parameters (spatial homogeneity of the static magnetic field in the MRI, echo time…). Modeling of inhomogeneous magnetic susceptibility field variations upon motion in-vivo is difficult and its feasibility remains unproven for clinical application. Approaches described in this study allow to correct displacement-related errors in PRF based MR thermometry for periodic motions avoiding explicit modeling of the susceptibility field.

In order to correct artifacts generated in temperature maps by periodical organ motion, the perturbation of phase images upon motion is analyzed during a pretreatment procedure. This step is performed prior to the therapeutic intervention without hyperthermia. An atlas of motion is constructed with MR images acquired during this pretreatment period (28,29). For that purpose, 50 images are acquired to sample the periodical motion. The reference anatomical image for motion estimation for the image registration algorithm is chosen to be the first one in the temporal series. During the pretreatment step, anatomical images are stored in the atlas with the corresponding phase image. Then, during the thermal therapy, each time a new data set is available, the current anatomical image is compared to anatomical images stored in the atlas using an inter-correlation coefficient. The anatomical image of the atlas with highest similarity is selected, and the corresponding phase image is used as the reference for temperature computation. Finally, the motion field vector estimated from anatomical images is used to correct the spatial transformation in the obtained temperature map.

Adjustment of focal point position taking during periodical organ motion

During an intervention on a mobile organ, the focal point position should be adjusted in order to focus the targeted area initially defined by the radiologist. Target displacements due to periodical motions require a continuous focal point adjustment. Note that the position estimated on the last acquired image is different with respect to the actual tissue position due to a time delay. This delay between the real displacement of the target and the availability of motion information is composed of time periods needed for acquisition, reconstruction, transfer and processing (thermal map computation, motion estimation) of the data. As implementated in this study, the delay is close to 2 s and thus cannot be neglected. If uncorrected, with a typical period of the human respiratory cycle of approximately 5 s, the estimation of the focal point displacement would be close to an opposition phase with respect to the actual target position. Thus, the error in the focal point positioning may increase by a

factor of almost two. In addition, the interval of time for data transfer between the MRI and the HIFU computer may be variable resulting in random temporal variations of the estimated period of the motion. For the reasons above, the target displacement must be anticipated with a delay which must be quantified. The criterion used for this anticipation is based on an analysis of the main global motion variation detected in the MR images. This average displacement offers the advantage to be stable against noise because it is computed from all image voxels. A motion atlas is built from motion field vectors computed during a pretreatment step. Each field is associated to the corresponding main global motion.

The motion anticipation requires several steps:

1. *Estimation of the typical period of the motion*

An analytic model of the main global motion is defined at the end of the pretreatment step in order to provide during the intervention: 1) a temporal localization of the displacement in the typical period estimated from the current dynamic, 2) a mathematical anticipation of future displacements until the acquisition of the next dynamic.

Due to possible irregularities of the respiratory cycle, an average of the period duration is evaluated during the pretreatment step to define the duration of a typical period. The pretreatment step covers several periods, which are not necessarily identical. To maintain the method compatible with variable respiratory cycle, all sampled periods of the pretreatment step are projected onto an average period. This procedure leads to a densely sampled average period. This main periodical motion M is described with the N^{th} order Fourier decomposition:

$$M(t) = \sum_{n=0}^{N} a_n \cdot \cos(n\omega t) + b_n \cdot \sin(n\omega t) \qquad [3]$$

In this equation a_n and b_n correspond to harmonic values. In practice, N=3 is found to be a good compromise to get an efficient typical period model. Higher harmonics correspond to amplitudes lower than 0.1 mm.

Coefficients a_n and b_n are computed from a least square approximation method with P points acquires during the pretreatment step as follow:

$$a_n = \frac{\sum_{i=1}^{P} M(t_i)\cos(n\omega t_i)}{\sum_{i=1}^{P} \cos(n\omega t_i)^2} \quad \text{and} \quad b_n = \frac{\sum_{i=1}^{P} M(t_i)\sin(n\omega t_i)}{\sum_{i=1}^{P} \sin(n\omega t_i)^2} \qquad [4]$$

2. Current phase within the estimated motion

To determine the temporal point t_i of an image with an estimated main displacement D in the typical period, the equation $D=M(t_i)$ must be solved. However this equation leads to several solutions. A non-determination subsists between increasing and decreasing parts of the cycle. The history of motion is used to solve this ambiguity. For that, an Euclidian distance is computed between the L^{th} last main displacements (in this study L has been set to 5) and the trigonometric polynomial function. This method provides accurate and stable temporal localization of acquired dynamics in the typical period.

3. Anticipation of the displacement

With the knowledge of time t_i and compensating delay measured by the microcontroller, the real target displacement can be deduced from the model $M(t)$. Future displacements are also computed with a temporal resolution of 100 ms. 15 displacements are predicted in order to provide enough anticipated displacements until the treatment of the next dynamic. Displacement is anticipated for a delay of 1.5 s. This provides a margin on transmission jitter of 0.5s taking into account that the dynamic duration is set to 1 s.

With a translational motion along a single axis, knowledge of the main global motion suffices to determine the displacement of the complete target. For complex motions, the image in the atlas with the closest main global motion is used to select the corresponding motion field.

Automatic temperature control in mobile target

Temperature control in a single HIFU focal point

In a single point, the temperature can be adjusted from MR thermal map (18,19,20)**,** by a proportional, integral and derivative control using a controller. This technique is based on the differential equation [5] including proportional, derivative and integral terms to minimize the temperature error ξ,

R1.8

$$\frac{\partial \xi}{\partial t} + a\,\xi + \frac{a^2}{4}\int_0^t \xi = 0 \quad \text{with} \quad \xi = \theta - T \qquad [5]$$

The parameter ξ represents the difference between the target temperature θ and the measured temperature T, the proportional control (second term) is equal to the instantaneous error between the measured and the targeted temperature, the integral control (third term) is defined by the sum of the past temperature errors, and the derivative control (first term) is determined by the present temperature variation in order to reach the future target temperature.The parameter a can be defined by the operator and influences the relative importance of the three contributions in a PID controller. This automatic control ensures a stable convergence to the target temperature.

The proportional, integral and derivative control is also combined with the bioheat transfer equation [6] in order to anticipate the tissue reaction. This equation takes into account the thermal diffusion coefficient D, the ultrasound absorption of the tissue α and the ultrasound power intensity P.

$$\frac{\partial T}{\partial t} = D \cdot \nabla^2 T + \alpha \cdot P \qquad [6]$$

The PID differential equation is respected if the power is set to the value defined by the expression [7] which adjusts correctly the derivative term:

$$P = \frac{1}{\alpha}\left[\frac{\partial T_C}{\partial t} - D \cdot \nabla^2 T + a(\theta - T) + \frac{a^2}{4}\int_t (\theta - T)\right] \qquad [7]$$

To control the temperature in a voxel of mobile tissue, the PID feedback loop algorithm is computed from the corrected thermal map which is registered to a central reference position. With those thermal maps all computations concerning required power for temperature control are carried out in the same way as for statictissue. After required power determination, the position of the focal is adjusted every 100 ms with the anticipation motion algorithm previously described.

Spatial temperature control

R1.9

To treat a large volume of several milliliters with a small focal point volume of only one cubic millimeter, a proposed solution is to move the focal point along a trajectory (21, 32). To spatially control the temperature, the amount of applied acoustical power is defined by equation [7] for all points of the targeted volume However , whatever the type of technology used to displace the focal point (electronic or mechanical), it is technically difficult to emit this defined power simultaneously into each point. To avoid this problem, the

amount of energy E deposed during one feedback cycle t_F into the point r is defined by equation [8].

$$E_{(\vec{r})} = \frac{t_F}{\alpha}\left[\frac{\partial\theta_{(\vec{r})}}{\partial t} - D\cdot\nabla^2 T_{(\vec{r})} + a\left(\theta_{(\vec{r})} - T_{(\vec{r})}\right) + \frac{a^2}{4}\int_t\left(\theta_{(\vec{r})} - T_{(\vec{r})}\right)\right] \quad [8]$$

This energy is delivered successively into every point, choosing the appropriate duration and power (21). Points requiring high energy value are heated preferably with a long duration rather than high power intensity for improved safety. Therefore, the feedback cycle time is divided into several durations with a weighting corresponding to the needed energy in order to limit maximal power emission. To optimize the quality of temperature control, the feedback cycle is set to the shortest possible value which is equal to the duration of one dynamic (1 s in this study).

This control method assumes that there is no energy interaction between successive ultrasound beams for the different focal point locations. In a plane perpendicular to the beam axis, this hypothesis is valid when secondary lobes are negligible. Along the beam axis there is an overlap of the acoustic field of the different focal point locations. This overlap tends to produce an elongated heated volume along the beam axis depending on focal point distance and the transducer aperture angle. To avoid having to take into account such overlap in the feedback algorithm, the temperature control has been limited to a coronal slice perpendicular to the vertical beam axis (21). In addition, the temperature increase produced in adjacent parallel slices is inferior to the temperature in the controlled region corresponding to a linear (and not a surface) heating trajectory.

R1.9

The spatial feedback temperature control is also computed with corrected and registered thermal maps. The trajectory provided by this feedback algorithm is modified in order to force focal points to track the target. Each point of this trajectory is split in a succession of several points with durations close to 100 ms. After splitting, those points are translated with a shift defined by the anticipated motion. As a result, the energy defined by the spatial temperature control algorithm is deposited with a high sampling rate.

Results

To test the efficiency of the proposed method, ex-vivo muscle was heated with a HIFU transducer placed below the evaluation platform during successive applications of periodical rigid and elastic motion.

R2.19

Periodical rigid motion

Ex-vivo muscle was displaced with a periodical translational motion of 14 mm with a duration of 5.6 s. The muscle was heated with HIFU emitting 24 Watt acoustical, during 1 minute. Figure 2 gives a comparison of temperature maps (during the heating) and the thermal dose maps (at the end of the experience) between studies realized with and without thermal artifacts and focal point position correction. Temperature errors are reduced from 40 °C to lessthan 1 °C when the thermal correction is applied making focal point localization and thermal dose computation possible. Without focal point position correction, the heating area is spread along 14 mm length and the induced heating does not lead to tissue ablation as temperature increase is insufficient. On the other hand, with correct focal positioning, the heating pattern is circular and the energy is deposited over the same tissue area leading to necrosis.

Periodical elastic motion

The more frequent and complex case to correct for is periodical elastic motions. To mimic those displacements, ex-vivo muscle tissue was submitted to elastic periodical motion with a period duration close to 5.6 s. The muscle has been heated by HIFU emitting a power of 100 electrical watts during 1 minute. Figure 3 shows anatomical images obtained at different positions in the cycle with the corresponding field vector displacements estimated with a centered reference image. Figure 4 provides a comparison between temperature maps (during the heating) and thermal dose maps (at the end of the experience) obtained with and without thermal and focal point position correction.Temperature errors without thermal correction can reach 300 °C in one minute. Phase variations greater than 2π between two dynamics induce an accumulated thermal error which increases during the heating. Similar to experiments described above, thermal dose maps obtained without thermal correction are unusable. Without focal point position correction, the heating area is spread along a 12 mm trajectory and the induced heating does not lead to tissue ablation as temperature increase is insufficient. With correct focal positioning, the heating pattern is circular and the energy is deposited over the same tissue area leading to necrosis.

Temperature control with motion tracking

The heating procedure with the focal point position correction, described previously, provides a temperature increase with a constant power deposition in the same target point despite tissue motion. Those correction methods also provide good temperature maps with a quality close to the maps acquired without motion. Thus, the corrected temperature maps may be used to control temperature. PID feedback loop algorithms were applied to an ex vivo muscle tissue undergoing a periodical translation.

Figure 5 shows a comparison between two heating procedures realized with spatial temperature control of immobile tissue (5a and 5c) or undergoing periodical rigid motion (5b and 5d). The amplitude of the motion has been set to 8 mm along the Z axis in order to maintainthe possibility to move the focal point 9 mm along the perpendicular axis X. According to those amplitudes, the focal point does not deviate more than 6 mm from the central point. With a voxel width of 1.5 mm, the temperature control was achieved over 7 central voxels to obtain a linear heating segment of 9 mm. Light grey, dark grey and black solid curves on graphs 5a and 5b represent minimal, average and maximal temperature, respectively, for those 7 voxels compared to dashed curves representing the targeted temperature. Light grey, dark grey and black solid curves on graphs 5c and 5d represent temperature measures along this segment at three different time points during the temperature increase. Light grey, dark grey and black dot curves describe the corresponding target temperature increase.

The actual temperature increase corresponds to the targeted temperature increase with an accuracy of 0.5 °C over the entire heating segment. The average difference between the maximal and the minimal temperature was 1.2 °C for the study with immobile tissue and 1.3 °C with mobile tissue. With the motion tracking technique, tissue displacements did neither induce any significant noise in temperature maps nor lead to any measurable loss of precision in temperature control. Figure 6 shows a comparison of temperature maps acquired at 141 s and 215 s obtained ex-vivo with immobile and muscle undergoing periodical rigid motion in the direction top-to-bottom of Figure 6. The elongated segment of 9 mm along the X axis appears clearly as if the tissue moved along the perpendicular direction with an amplitude of 8 mm. The straight segment shapes confirm that focal point motion tracking was achieved correctly.

Since the focal point position is adjusted as a function of the tissue displacement, the temperature control accuracy only depends on feedback algorithm performance. Because the differential equation [5] of the PID controller gives a dual solution of a/2, the response time of

R1.10

the system is equal to 2/a. To avoid temperature control instability induced by system latency around 2 s (measurement, transfer and analysis delay), the response has been set to the duration of 8 s.

Precision of the tracking method proposed for periodical motions

To evaluate the performance of the correction method, it is interesting to compare the estimated displacement from MR images and the anticipated displacement with the real displacement of the target measured by a microcontroller via a striped bar placed on the transmission line.

Approach used for rigid periodical motions correction

For stable motion compensation, it is necessary to update the anticipated displacement as often as possible. The anticipated displacement is updated at each acquired dynamic with a measurement of the delay to compensate. This delay is mainly composed of the dynamic acquisition duration (1 s), the transmission and the processing delay which varies from 0.3 s to 1.1 s, with an average value of 0.9 s. This variation of the availability of motion information depends on the operating system used. In the example shown this was carried out under Windows XP (not a real time Operating System). The delay was measured directly with a microcontroller keeping time between the beginning of the acquisition of the last dynamic (external pulse provided by the image reconstructor) and the end of the corresponding processing. Figure 7 describes results obtained with an anticipated motion, updated at each dynamic based on this measured delay. Those results correspond to the study with a periodical translational motion reported in Figure 2c and 2f. The method is shown to be efficient since the standard deviation between the measured and the anticipated motion remains constant close to 0.3 mm in the experiment reported in Figure 2. The anticipated motion is a continuous curve except for infinitesimal discontinuities matching the periodical target motion.

To evaluate precisely the accuracy and the reproducibility of the target position anticipation process, this experiment was repeated 14 times. The average error and standard deviation over all studies was 0.33 ± 0.03 mm, respectively. The minimal and maximal errors evaluated over one period were 0.26 mm and 0.45 mm, respectively.

R2.18

R1.11

Approach used for correction of elastic periodical motions

For elastic deformations, the main displacement was insufficient to characterize the estimated motion of the target. Moreover, the displacement measured with the transmission line is not enough to characterize the target point in the tissue and can not be compared to the motion tracking for elastic motions reported in Figure 3. To correct for elastic motions, the main displacement was used as a criterion to select appropriate field vectors in the atlas. Therefore, to quantify this lack of performance, the anticipated motion obtained when the atlas technique was applied to a periodical translational motion similar to the previous one was compared to the motion measured by the striped bar. The anticipated displacement was sampled with 50 values corresponding to the 50 field vectors stored in the atlas. This sampling of the anticipated motion decreased slightly the accuracy of the motion determination. The error between the real and the anticipated motion was close to 0.4 mm (average over 4 experiments) as compared to 0.3 mm obtained previously using rigid body motions.

Discussion

The use of phased array transducer technology allows very fast electronical displacement of focal point. The transducer with 256 elements of 6 mm diameter used in this study allowed a displacement of 15 mm at 1.5MHz. This amplitude offers the possibility to correct most of the displacements in organs under respiratory motion. The described motion correction methods can be directly generalized for three-dimensional motions. Results described in this study are two-dimensional because of limitations imposed by transmission of data between MRI computer and HIFU computer.

Signal localization errors may be caused by instrumental imperfections and/or limitations. Some localization errors can also be induced by the imaged object, like susceptibility artifact for paramagnetic material or chemical shift for a specific water and fat composition. As a result, geometric distortions in modulus and phase images modify anatomical images and estimated motions. Those artifacts can be limited with an optimal MR acquisition sequence or corrected with specific correction processes (33).

Focal point position correction upon organ displacement is necessary for treatment of a mobile target. However, in case of MRI guidance a delay in execution of the correction

cannot be avoided. Before an image is available, there is an acquisition, transmission and calculation delay close to 2 s. During this duration the position of the focal point is not yet updated. For periodical motions, the correction technique described is limited to motion with a period duration larger than the acquisition duration. According to the Shanon- Nyquist theorem, the sampling requires at least 2 dynamics per period to reconstruct a typical period model In the studies shown, the motion period duration was 5.6 s and the dynamic acquisition duration was 1s, sufficient to obtain good period reconstruction.

Displacements applied to correct motion artifacts are limited to displacements detected during pretreatment step. This limitation of motion sampling may be avoided using interpolation of detected displacement.

Analysis of the precision of the focal point repositioning

Without displacement correction, the average error of the focal point position was measured experimentally at 4.8 mm. A theoretical estimation of this error can be calculated with a first harmonic approximation of the real motion. Equation [3] leads to

$$M(t) \approx c_1 \cdot \cos(w\,t) \quad \text{with} \quad c_1 = \sqrt{a_1 + b_1} = 6{,}5\,mm \quad \text{and} \quad T = \frac{2\pi}{\omega} = 5{,}6\,s \qquad [9]$$

with c_1 indicating the amplitude of the first harmonic and using the definition of a and b as in Equation 3. The theoretical error induced by this motion is:

$$\sigma_{\text{without correction}} = \sqrt{\frac{1}{T}\int_0^T \left(c_1 \cdot \cos(w\,t)\right)^2 \, dt} = \frac{c_1}{\sqrt{2}} = 4{,}6mm \qquad [10]$$

When the focal point was repositioned with the displacement estimated from the last available image but without taking into account the anticipated displacement during the delay following the last available image, the average experimental error was 7.54 mm. The theoretical estimation of this error might be quantified by supposing that the delay to be compensated is constant (d_C=1.9 s). The difference in phase induces is equal to φ_C:

$$\varphi_C = 2\,\pi\,\frac{d_C}{T'} = 2{,}1\,rad = 120° \qquad [11]$$

The theoretical error induces by this phase difference is:

$$\sigma_{without\ anticipation} = \sqrt{\frac{1}{T}\int_0^T \left(c_1 \cdot \cos(w\,t) - c_1 \cdot \cos(w\,t + \varphi_C)\right)^2 \, dt} = c_1 \cdot \sqrt{2} \cdot \left|\sin\frac{\varphi}{2}\right| = 8mm \qquad [12]$$

When the delay to be compensated is correctly measured, the experimental error measured is 0.3 mm with rigid motion algorithm and 0.4 mm with elastic motion algorithm. Theoretically, there is no phase difference between the anticipated and the real displacement, therefore this error should be 0. Table 1 showsa comparison of the theoretical and experimental standard deviations obtained with each approach for the periodical translation motion. The anticipated motion is shown to provide an accurate focal point repositioning, 14 times better as compared to positioning without motion correction.

Stability of the displacement correction in case of motion periodicity variations

The duration between the localization of the current dynamic in the typical period model and the required anticipation time is composed of:

- The localization process of a dynamic within the motion cycle. This step required a windowing of L dynamics. The average delay induced is equal to $(L-1)/2$ dynamics duration.
- The delay to compensate which is composed of the acquisition, transmission and processing duration of one dynamic.
- The anticipation of the trajectory until the next dynamic acquisition. The average of this delay is equal to half a dynamic duration.

This duration corresponding to the system response delay d_R is thus equal to 2+1.9+0.5=4.4 s. The periodical motion hypothesis is not perfectly respected in practice because of variations in physiological cycle. Therefore, the period duration may change during the intervention. This induces an error in motion anticipation. If the period motion duration is equal to T, the anticipated motion is calculated with a phase shift equal to $\varphi = 2\pi \cdot d_R/T$. On the other hand, if the period duration becomes T', the phase shift required is $\varphi' = 2\pi \cdot d_R/T'$. However, the anticipated motion is still computed with a phase shift φ instead of φ'. Therefore, the phase difference between the anticipated motion with a period duration T and the real motion with a period duration T' is $\Delta\varphi$:

$$\Delta\varphi = \varphi' - \varphi = 2\,\pi\,d_R\left(\frac{1}{T'} - \frac{1}{T}\right) \qquad [13]$$

In this case, the standard deviation between the real and the anticipated motion is:

$$\sigma_{anticipation} = c_1 \cdot \sqrt{2} \cdot \left|\sin\frac{\Delta\varphi}{2}\right| \qquad [14]$$

To study the robustness of the proposed correction method, several tests were carried out with a period duration motion change of ±1 s with respect to the initial period of 5.6 s. Figure 8 compares the experimental standard deviation measured with a modification of the period duration and the theoretical standard deviation as described in Equation [14]. It can be seen that a standard deviation of 1.5 mm (corresponding to the width of a voxel) is obtained when the period variation does not exceed ±7%. The stability of this method against variation of period duration is proportional with the following parameters: i) the system response delay, ii) the motion amplitude, iii) the estimated period during the pretreatment step. In the general case of periodical motion with n harmonics the accuracy of the anticipated displacement is described by this expression

$$\sigma_{\text{anticipation}} = \sum_{n=0}^{N} c_n \cdot \sqrt{2} \cdot \left| \sin \; n \cdot \frac{\Delta\varphi}{2} \right| \quad \text{with} \quad c_n = \sqrt{a_n^2 + b_n^2} \qquad [15]$$

where c_n indicates the amplitude of the nth harmonic, and the definition of a and b as in Equation 3.

Precision of reported results

The uncertainty of reported results depends on the estimated motion method used and the accuracy of the evaluation platform. The two main sources of uncertainties induced by the platform are:

- The striped bar details the position of the transmission line with an accuracy of 0.5 mm. However, intermediate values are computed with a linear interpolation from the detected position.

- The mechanical connection between the transmission line and the ex vivo muscle is not perfectly rigid because of external friction. Those frictions may cause an estimated error of 0.5 mm of at each change of motion direction.

In fact, the actual standard deviation between the anticipated and the real motion is expected to be significantly lower than the value of 0.3 mm measured with this evaluation platform.

Conclusion

Correction methods for displacement artifacts in temperature maps of mobile targets may reduce temperature errors from several hundred degrees to values lower than one degree.

The techniques proposed here provide correction of focal point position for periodical complex motions (rigid or elastic). The correction of focal point position is accurate with a standard deviation error lower than 0.3 mm for the studies reported here. The temperature increase obtained for MR-HIFU with this correction is more efficient and correctly localized despite target displacements. Also, it is shown here that MR-HIFU heating with motion tracking is possible with spatial temperature control. This may provide tissue ablation without damaging neighboring tissue during motion.

The presented methods have been tested for two dimensional motions and can be generalized for three dimensional motions. The proposed techniques appear stable enough to treat organs like kidney or liver with MR-HIFU for a patient under respiratory control. For patient under free breathing, the system response delay should preferably be further decreased.

Real time information like respiratory gating, navigator echo or ultrasound echo (34) may be used instead of main global motion as a selection criterion for displacement field in the atlas. With further acceleration of motion tracking data, the stability is expected to be improved further because the anticipation delay will be reduced correspondingly.

References

(1) Lele PP, Production of deep focal lesions by focused ultrasound current status. Ultrasonics, 1967, vol. 5, pp. 105-112.

(2) Fry WJ, Tucker D, Fry FJ and Wulff VJ. Physical Factors Involved in Ultrasonically Induced Changes in Living Systems: I1 Amplitude Duration Relations and the Effect, of Hydrostatic Pressure for Nerve Tissue, J . Acoust. Soc. Am. 23, 364-368, 1951.

(3) Stewart EA, Rabinovici J, Tempany CMC, Inbar Y, Regan L, Gastout B, Hesley G, Kim HS, Hengst S, and Gedroye WM. Clinical outcomes of focused ultrasound surgery for the treatment of uterine fibroids. Fertility and Sterility 2006;85 (1):22-29.

(4) Furusawa H, Namba K, Thomsen S, Akiyama F, Bendet A, Tanaka C, Yasuda Y, and Nakahara H. Magnetic resonance-guided focused ultrasound surgery of breast cancer: reliability and effectiveness. J.Am.Coll.Surg. 203 (1):54-63, 2006.

(5) Pernot M, Aubry JF, Tanter M, Thomas JL, and Fink M. High power transcranial beam steering for ultrasonic brain therapy. Phys.Med.Biol. 48 (16):2577-2589, 2003.

(6) Dun F, Physical mechanism of the action of intense ultrasound on tissue. Ultrasonic Biophysics, 1976, 310-313.

(7) Pon JB, The role of heat in the production of ultrasonic focal lesions. Ultrasonic Biophysics, 1976, 347-351.

(8) Cline HE, Hynynen K, Hardy CJ, Watkins RD, Schenck JF, Jolesz FA. MR temperature mapping of focused ultrasound surgery. Magn Res. Med. 1994;31:628-636.

(9) Wlodarczyk W, Boroschewski R, Hentschel M, Wust P, Monich G, Felix R. Three-dimensional monitoring of small temperature changes for therapeutic hyperthermia using MR. J. Magn. Res. Imaging 1997;7:918-928

(10) Hynynen K, McDannold N, Clement G, Jolesz FA, Zadicario E, Killiany R, Moore T, and Rosen D. Pre-clinical testing of a phased array ultrasound system for MRI-guided noninvasive surgery of the brain-A primate study. Eur.J.Radiol., 2006; 59(2):149-56.

(11) Kennedy JE, ter Haar GR, and Cranston D. High intensity focused ultrasound: surgery of the future? Br.J.Radiol. 76 (909):590-599, 2003.

(12) Hynynen K, Pomeroy O, Smith DN, Huper PE, McDannold NJ, Kettenbach J, Baum J, Singer S, Jolesz FA. MR imaging-guided focused ultrasound surgery of fibroadenomas in the breast: a feasibility study. Radiology 2001;219:176-185.

(13) Zippel DB, Papa MZ, The use of MR imaging guided focused ultrasound in breast cancer patients; a preliminary phase one study and review. Breast Cancer 12 (1):32-38, 2005.

(14) Tempany CM, Stewart EA, McDannold N, Quade BJ, Jolesz FA, Hynynen K. MR imaging-guided focused ultrasound surgery of uterine leiomyomas: a feasibility study. Radiology. 2003 Mar;226(3):897-905.

(15) Elizabeth A Stewart, Jaron Rabinovici, Clare MC Tempany, Yael Inbar, Leslie Regan, Bobbie Gastout, Gina Hesley, Hyun S. Kim, Suzanne Hengst, and Wladyslaw M. Gedroye. Clinical outcomes of focused ultrasound surgery for the treatment of uterine fibroids. Fertility and Sterility 85 (1):22-29, 2006.

(16) Guilhon E, Quesson B, Moraud-Gaudry F, de Verneuil H, Canioni P, Salomir R, Voisin P, Moonen CTW. Image-guided control of transgene expression based on local hyperthermia. J. Molecular Imaging, 2(1):11-7, 2003.

(17) McDannold N, Fossheim SL, Rasmussen H, Martin H, Vykhodtseva N, and Hynynen K. Heat-activated liposomal MR contrast agent: initial in vivo results in rabbit liver and kidney. Radiology 230 (3):743-752, 2004.

(18) Vimeux FC, de Zwart JA, Palussière J, Fawaz R, Delalande C, Canioni P, Grenier N, Moonen CTW, Real-time control of focused ultrasound heating based on rapid MR thermometry. Invest. Radiol. 1999; 34, 190-193.

(19) Salomir R, Vimeux F, de Zwart JA, Grenier N, Moonen CTW, Hyperthermia by MR-Guided Focused Ultrasound: Accurate Temperature control Based on Fast MRI and a Physical Model of Local Energy Deposition and Heat Conduction. Magnetic Resonance in Medicine 2000; 43:342-347.

(20) Quesson B, Vimeux F, Salomir R, de Zwart JA, Moonen CTW, Automatic Control of Hyperthermic Therapy Based on Real-Time Fourier Analysis of MR temperature Maps. Magnetic Resonance in Medicine 2002:47;1065-1072.

(21) Mougenot C, Salomir R, Palussière J, Grenier N, Moonen CTW, Automatic Spatial and Temporal Temperature Control for MR-guided Focused Ultrasound Using Fast 3D MR Thermometry and Multispiral Trajectory of the Focal Point, Magnetic Resonance in Medicine 2004; 52:1005-1015.

(22) Hindman J. Proton resonance shift of water in the gas and liquid states. J Chem Phys 1966 ;44 :4582-4592.

(23) Ishihara Y, Calderon A, Watanabe H, Okamoto K, Suzuki Y, and Kuroda K. A precise and fast temperature mapping using water proton chemical shift. Magn.Reson.Med. 1995; 34 (6):814-823.

(24) De Poorter J, De Wagter C, De Deene Y, Thomsen C, Stahlberg F, and Achten E. Noninvasive MRI thermometry with the proton resonance frequency (PRF) method: in vivo results in human muscle. Magn Reson.Med. 1995; 33 (1):74-81.

(25) Sapareto SA, Dewey CW. Thermal dose determination in cancer therapy, Int J Rad Oncology Biol Phys 1984, 10, 787-800.

(26) Hazle JD, Stafford RJ, Price RE. Magnetic resonance imaging-guided focused ultrasound thermal therapy in experimental animal models: correlation of ablation volumes with pathology in rabbit muscle and VX2 tumors. J Magn Res Imaging. 2002; 15 : 185-194.

(27) de Zwart JA, Vimeux F, Palussière J, Salomir R, Quesson B, Delalande C, and Moonen CTW, On-Line Correction and Visualiszation of Motion During MRI-Controlled Hyperthermia. Magnetic Resonance in Medicine. 2001; 45:128-137.

(28) Denis de Senneville B, Quesson B, Desbarats P, Salomir R, Palussière J, Moonen CTW, Atlas-Based Motion Correction For On-Line MR Temperature Mapping, IEEE, ICIP 2004; Singapore, vol. III, 2571-2574.

(29) Denis de Senneville B, Quesson B, Desbarats P, Mougenot C, Moonen CTW. Image processing for on-line reduction of thermometry artifacts, ISMRM, Seattle - Washington. 6-12 May 2006.

(30) Gavrilov LR, Hand WH, A theoretical assessment of the relative performance of spherical phased arrays for ultrasound surgery. IEEE Transactions on ultrasonics 2000 ; 47: 125-139.

(31) Salomir R, Denis de Senneville B, Moonen CTW. A fast calculation method for magnetic field inhomogeneity due to an arbitrary distribution of bulk susceptibility. Concepts

in Magnetic Resonance Part B (Magnetic resonance Engineering), Vol. 19B(1) 26-34. 7 July 2003.

(32) Lele PP. Induction of deep, local hyperthermia by ultrasound and electromagnetic fields: problems and choices. Radiat.Environ.Biophys. 1980; 17 (3):205-217.

(33) Schmithorst VJ, Dardzinski BJ, Holland SK. Simultaneous correction of ghost and geometric distortion artifacts in EPI using a multiecho reference scan. IEEE Trans Med Imaging. 2001 Jun;20(6):535-9.

(34) Pernot M, Tanter M, Fink M. 3D Real-time Motion Correction in High Intensity Focused Ultrasound Therapy. Ultrasound Medicine and Biology, 30(9):1239-1249, sept 2004.

(35) Friston KJ, Ashburner J, Frith CD, Poline JB, Heather JD and Frackowiak RSJ. Spatial registration and normalisation of images. Human Brain Mapping. 2:165-189. 1995.

(36) Wolberg G, Zokai S. Robust Image Registration Using Log-Polar Transform. Department of computer Science, City College of New York. 2000.

(37) Schunck BG, Horn KP. Determining optical flow. Artificial intelligence, 17:pp. 185-203,1981.

(38) Lucas B and Kanade T. An iterative image registration technique with an application to stereo vision. In Proceedings of the International Joint Conference on Artificial Intelligence, pp. 674- 679. 1981.

(39) Maintz JBA, Viergever MA. A survey of medical image registration, medical Image Analysis, vol. 2, number 1, pp 1-36, 1998.

(40) Barron J.L., Fleet D.J. and Beauchemin S.S., "Performance of Optical Flow Techniques", International Journal of Computer Vision, Vol. 12, No. 1, pp. 43-77, 1994.

Standard deviation	Without correction	Without anticipation	Translation motion	Elastic motion
Experimental	4.8 mm	7.5 mm	0.3 mm	0.4 mm
Theoretical	4.6 mm	8.0 mm	0.0 mm	0.0 mm

Table 1. Error of focal point position for different types of correction in mm.

R1.11

R1.12

List of figures

Figure 1. Mechanism used to displace the target in a cone-shaped piece of meat. The HIFU transducer is placed in the center of the magnet, and the motor at the end of the patient bed.

Figure 2. Temperature variation maps (a, b, c) and thermal dose maps (d, e, f) obtained ex-vivo during heating of pig muscle undergoing a periodical translation:

a and d: without thermal and focal point position correction,

b and e: with thermal correction but without focal point position correction,

c and f: with thermal and focal point position correction.

Figure 3. Anatomical images (a, b, c, d, e) acquired at different time periods during the periodic elastic motion and corresponding displacement field vectors (f, g, h, i, j) required for registering the anatomical image at the reference position.

Figure 4. Temperature variation maps (a, b, c) and thermal dose maps (d, e, f) obtained ex-vivo during heating of pig muscle undergoing an elastic periodical motion:

a and d: without thermal and focal point position correction,

b and e: with thermal correction but without focal point position correction,

c and f: with thermal and focal point position correction.

Figure 5. Spatial temperature control along a 9 mm line on immobile tissue (a, c) or tissue undergoing rigid periodical motion (b, d):

a and b: temporal temperature measurements,

c and d: spatial temperature measurements.

Figure 6. Temperature variation maps at 141 s (a, b) and 215 s (c, d) obtained ex-vivo during heating of pig muscle:

a and c: with immobilized muscle,

b and d: muscle tissue undergoing periodical rigid motion.

R2.16

Figure 7. Real (dotted line), estimated (dashed line) and anticipated displacement (solid line) measured with a periodical translational motion during 140s (a) or 20s after 2 minutes (b).

R2.21

Figure 8. Stability of the focal point position correction method as a function of the variation of the duration of the periodical motion for an anticipated delay of 4.4 s.

Appendix 1: Estimation of tissue displacement during motion

The proposed approach consists of using image processing techniques to estimate on-line organ displacements from anatomical images (28,29). Image registration allows organ displacement estimation with an excellent spatial resolution as compared to other existing approaches (34). The objective is to relate the coordinate of each part of tissue in the image to register with the corresponding one in a reference image. Here, the general principles are summarized.

In general, 3D vector field maps are preferred for this purpose. However, in practice it is difficult to acquire on-line 3D isotropic images because of the technical limitations and SNR associated with the fast 3D acquisition sequences. The approach used consists of estimating motion on 2D images generated by organs moving in 3D space. Image sections are oriented to include the principal axis of the organ displacement so that apparent movement is the best approximation of the real displacement. However, the presented algorithms may be implemented in the 3D case in order to estimate motion field between two volumes when technological progress will allow sufficient spatial and temporal resolution.

Let I_{ref} be the reference anatomical image (for example the first image of the time series) and I_{cur} the current image to register. I_{ref} and I_{cur} are two 2D normalized grayscaled images and the quantities $I_{ref}(x, y)$ and $I_{cur}(x, y)$ are the grayscale value of the two images at the coordinate (x, y) and the instant *t*. The objective is to relate the coordinate of each part of tissue in I_{cur} with the corresponding tissue in I_{ref}. A velocity field is extracted assuming that intensity is conserved during displacement. A general problem definition for image registration can then be expressed as follow: registering $I_{ref}(x, y)$ and $I_{cur}(x, y)$ is equivalent to estimating a coordinate transformation *T* that maximizes:

$$\max_{T} M\left(I_{ref}(x, y), I_{cur}\left(T(x, y)\right)\right)$$

where *M* is a criterion determining the accuracy of the registration.

R2.14

Registration efficiency is related to the nature and domain of the transformation to detect (global (35,36) or local (37,38) transformation). A compromise has thus to be found between the permissiveness of the spatial transformation *T* and the robustness of the estimation process. A well-adapted technique consists of using results obtained with a global transformation estimation as a starting point for a local transformation estimation. In this study, a global affine transformation is estimated in a first step, using a differential approach

of Gauss-Newton (35). In a second step, a hierarchical approach of Horn and Schunck algorithm (37) provides a good estimation of local organ displacements because of the regularity constraint assuming that motion field vectors have similar values for adjacent pixels matching real organ motion. Note that displacement estimation based on MR images allows sub-pixel accuracy as the registration process is computed with a large number of pixels.

Such image registration required 200 ms of computation time on our HIFU computer for one image of resolution 128×128 pixels. Further details can be found in references (39,40).

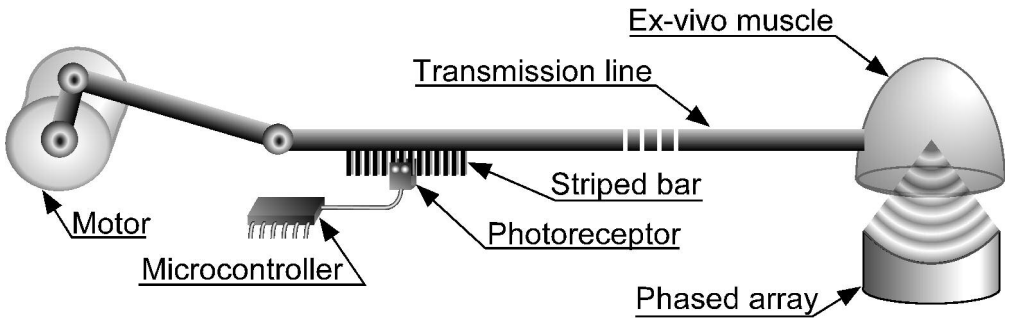

Figure 1. Mechanism used to displace the target in a cone-shaped piece of meat. The HIFU transducer is placed in the center of the magnet, and the motor at the end of the patient bed.

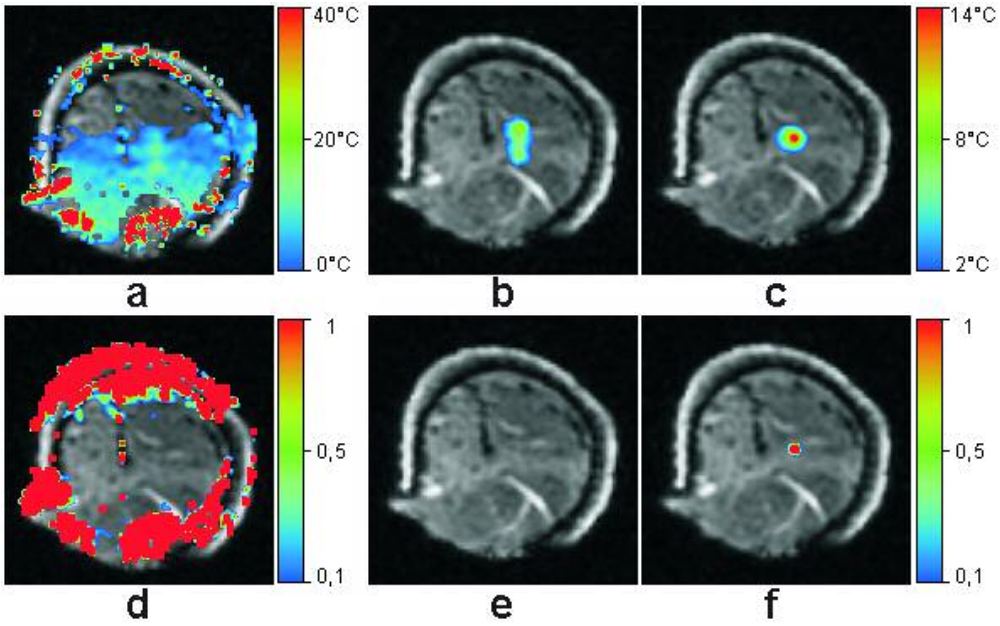

Figure 2. Temperature variation maps (a, b, c) and thermal dose maps (d, e, f) obtained ex-vivo during heating of pig muscle undergoing a periodical translation: a and d: without thermal and focal point position correction, b and e: with thermal correction but without focal point position correction, c and f: with thermal and focal point position correction.

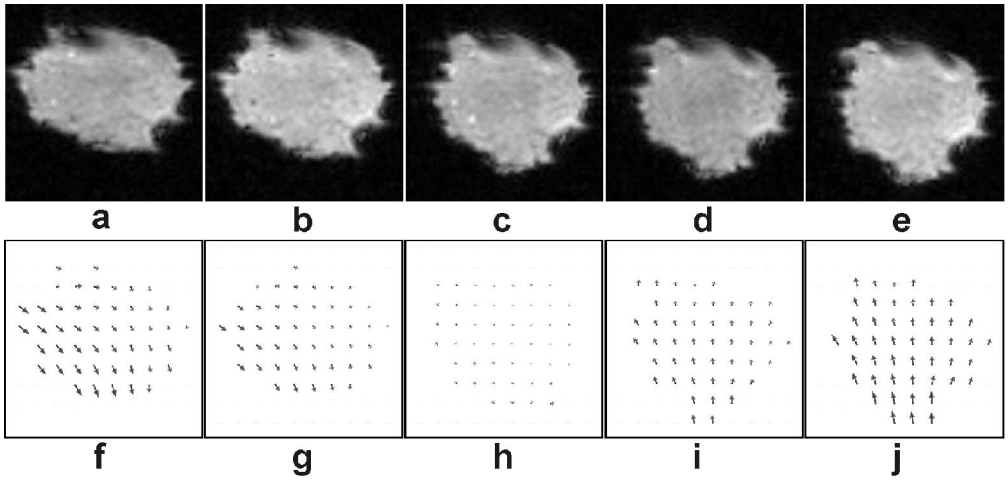

Figure 3. Anatomical images (a, b, c, d, e) acquired at different time periods during the periodic elastic motion and corresponding displacement field vectors (f, g, h, i, j) required for registering the anatomical image at the reference position.

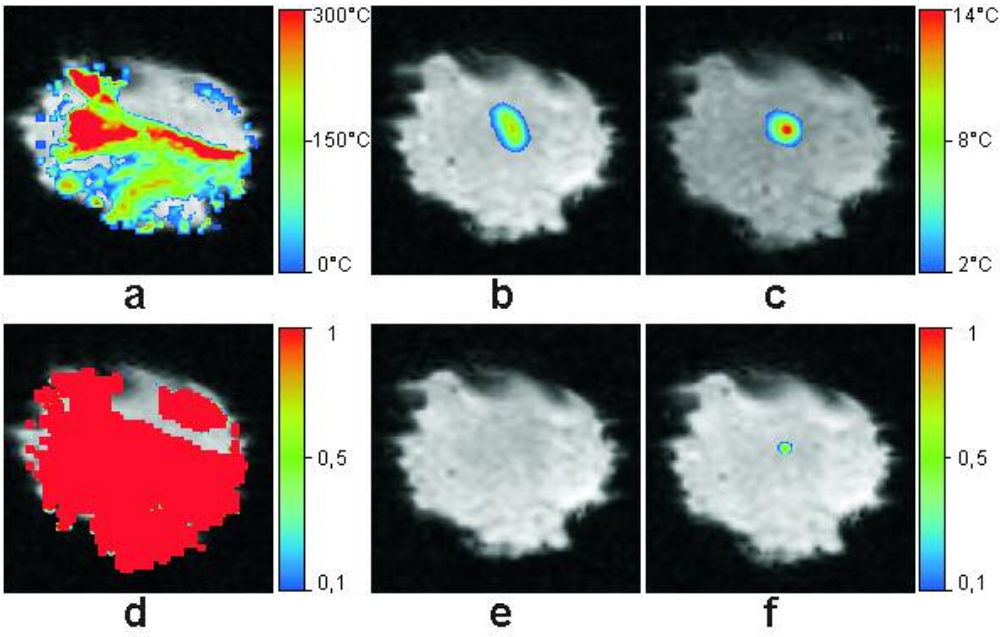

Figure 4. Temperature variation maps (a, b, c) and thermal dose maps (d, e, f) obtained ex-vivo during heating of pig muscle undergoing an elastic periodical motion: a and d: without thermal and focal point position correction, b and e: with thermal correction but without focal point position correction, c and f: with thermal and focal point position correction.

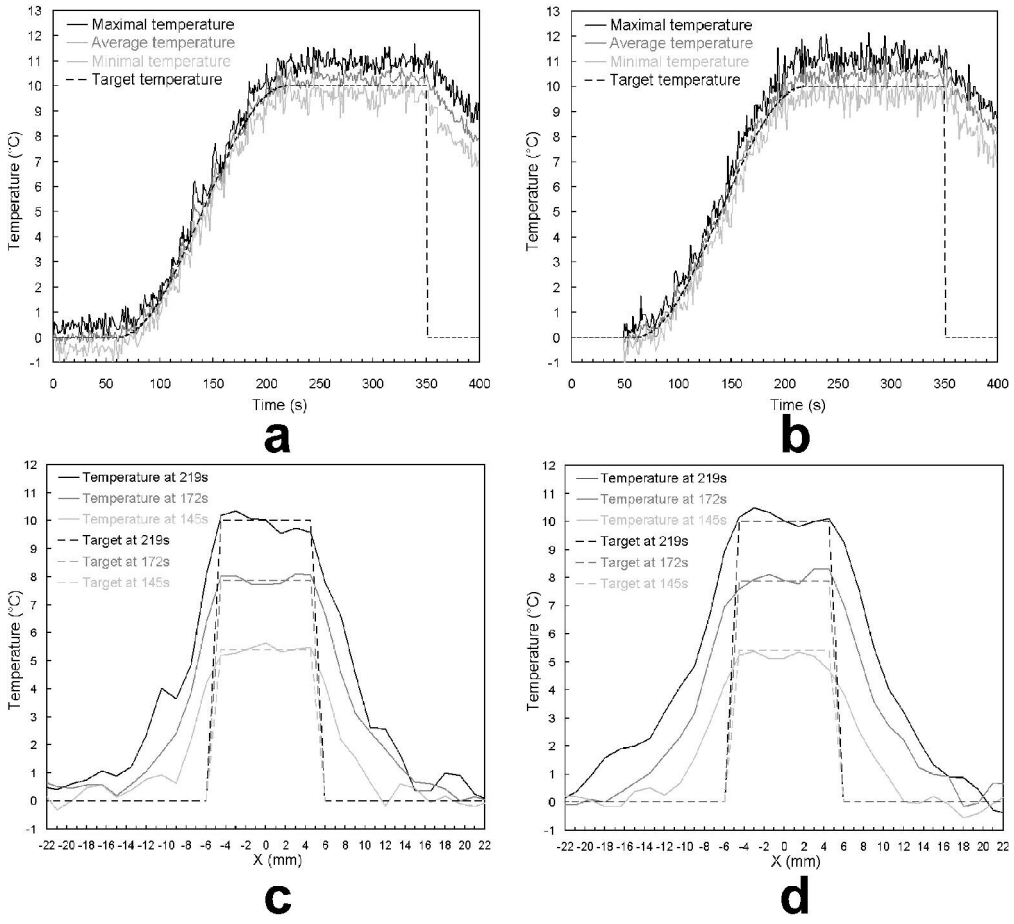

Figure 5. Spatial temperature control along a 9 mm line on immobile tissue (a, c) or tissue undergoing rigid periodical motion (b, d): a and b: temporal temperature measurements, c and d: spatial temperature measurements.

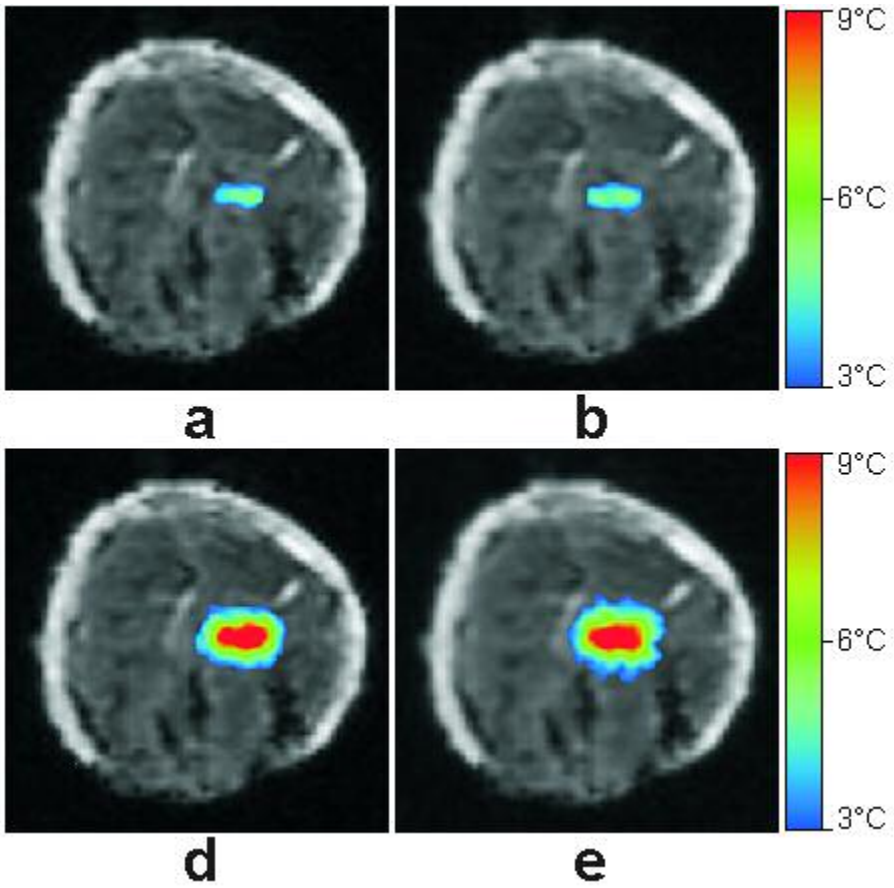

Figure 6. Temperature variation maps at 141 s (a, b) and 215 s (c, d) obtained ex-vivo during heating of pig muscle: a and c: with immobilized muscle, b and d: muscle tissue undergoing periodical rigid motion.

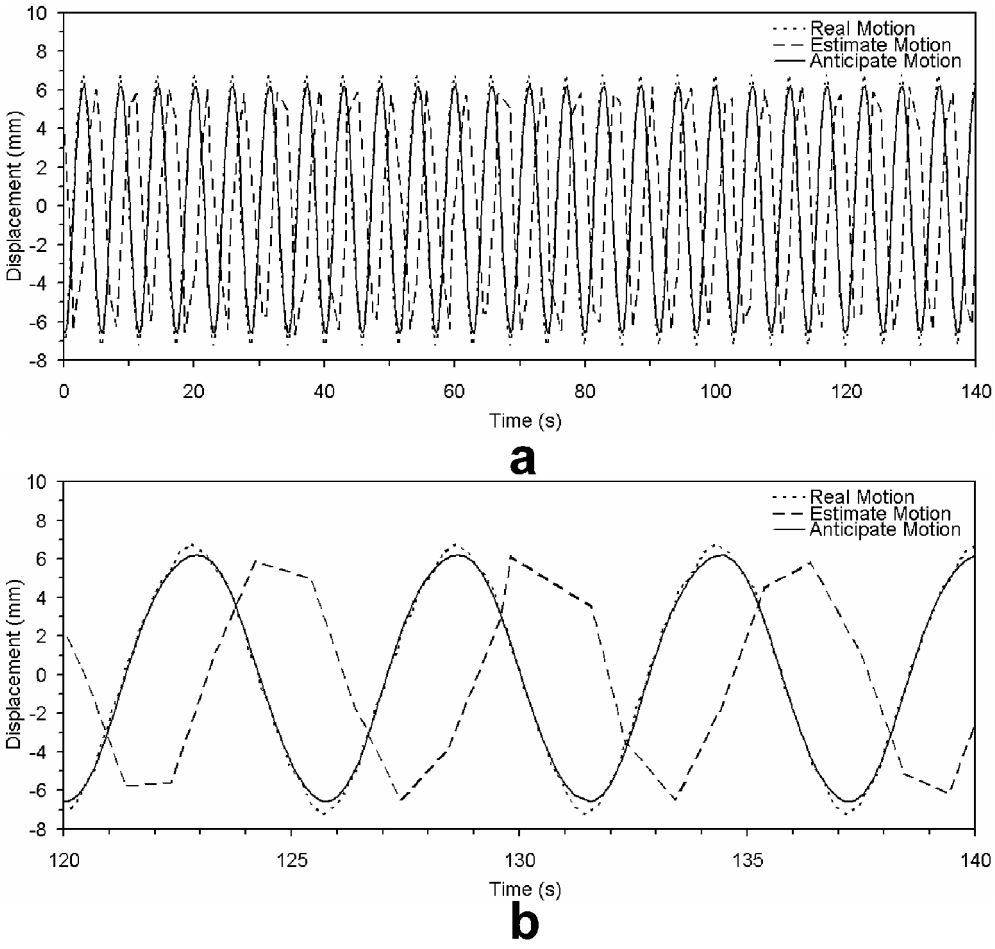

Figure 7. Real (dotted line), estimated (dashed line) and anticipated displacement (solid line) measured with a periodical translational motion during 140s (a) or 20s after 2 minutes (b).

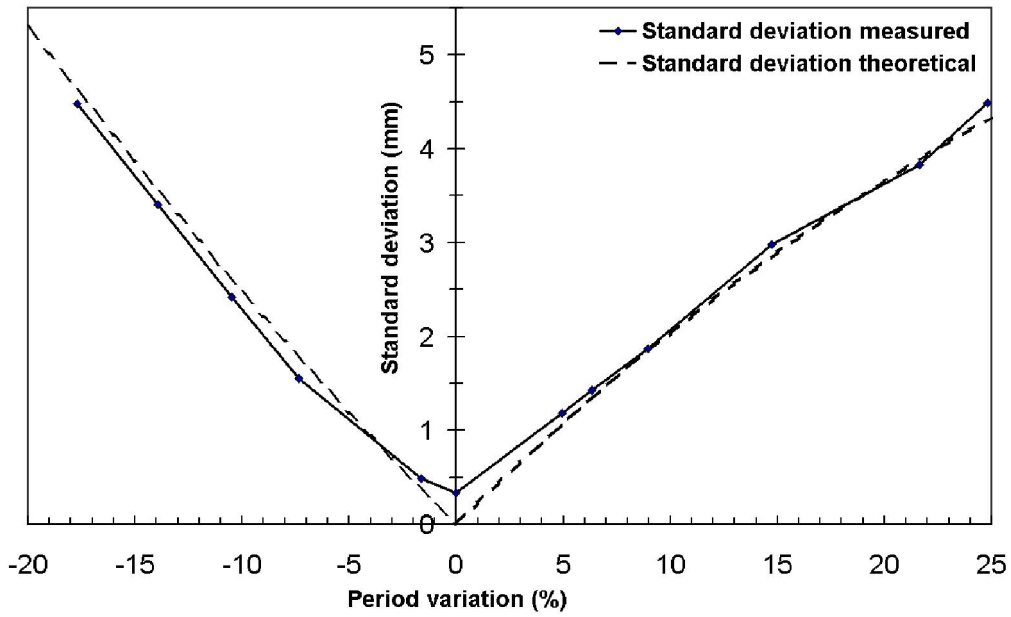

Figure 8. Stability of the focal point position correction method as a function of the variation of the duration of the periodical motion for an anticipated delay of 4.4 s.